Earth Planet. Sci. Lett. 681 (2026) 119930

Contents lists available at ScienceDirect

Earth and Planetary Science Letters

journal homepage: www.elsevier.com/locate/epsl

Triggering mechanisms of dynamic mass loss at a freshwater-calving glacier in southern Patagonia

Masahiro Minowa [a,*], Pedro Skvarca [b], Koji Fujita [c], Nozomu Naito [d], Shin Sugiyama [e,a]

[a] Institute of Low Temperature Science, Hokkaido University, Kita-19, Nishi-8, Kita-ku, Sapporo, 060-0819, Hokkaido, Japan
[b] Glaciarium—Centro de Interpretación de Glaciares, RP11, El Calafate, Z9405, Santa Cruz, Argentina
[c] Graduate School of Environmental Studies, Nagoya University, F3-1 200, Chikusa-ku, Nagoya, 464-8601, Aichi, Japan
[d] Faculty of Environmental Studies, Hiroshima Institute of Technology, 2-1-1, Mayake, Saeki-ku, Hiroshima, 731-5193, Hiroshima, Japan
[e] Arctic Research Center Hokkaido University, Kita-21, Nishi-11, Kita-ku, Sapporo, 001-0021, Hokkaido, Japan

ARTICLE INFO

Editor: J.P. Avouac

Keywords:
Calving glacier
Ice mass loss
Climate change

ABSTRACT

After quasi-steady state for a century, Glaciar Perito Moreno, a freshwater calving glacier in southern Patagonia, is showing signs of dynamic mass loss, beginning in 2018. We show that this recent dynamic ice mass loss was triggered by terminus retreat and ice thinning as a result of atmospheric warming, which overwhelmed stabilization due to morainal bank development. Beginning in 2018, thinning has spread over the lower part of the glacier, accompanied by gradual flow acceleration. The three seasons of pronounced melt years between 2020/21 and 2022/23 caused the glacier retreat from the moraine, resulting in substantial flow acceleration and thinning. Repeat lake depth measurements suggest that a decrease in water depth due to morainal bank growth and sedimentation, implying that the front was stabilized even under the warming of the prior decades. Our study highlights the complex behaviours of ice flow and frontal ablation on a freshwater calving glacier in relation to climate change.

1. Introduction

Glaciers are shrinking in reaction to anthropogenic climate warming with an accelerated rate in recent years (Rounce et al., 2023). Between 2000 and 2019, glaciers lost ~270 Gt yr^{-1} of ice mass, which is equivalent to ~20% of the global sea level rise during the same period (Hugonnet et al., 2021). The total mass loss from the glaciers is equivalent to that from the Greenland Ice Sheet and larger than that from the Antarctic Ice Sheet (Otosaka et al., 2023). The mass loss from the glaciers is anticipated to increase in this century, linearly with atmospheric warming (Rounce et al., 2023). The major uncertainty comes from the mass loss from calving glaciers, which flow into the ocean and lakes (Benn et al., 2007; Truffer and Motyka, 2016). Calving glaciers lose their mass not only on the surface in reaction to the atmospheric conditions, but also through iceberg calving and subaqueous melting at the front, collectively known as frontal ablation (Truffer and Motyka, 2016). Its variability is also highly dependent on ice dynamics, bed topography (e.g., Minowa et al., 2023a), moraine development (e.g., Eidam et al., 2020), atmospheric (e.g., Cowton et al., 2018), and aquatic conditions (e.g., Foss et al., 2024) at the terminus, hence its changes are sometimes independent of the climate condition (e.g., Brinkerhoff et al., 2017).

It has been reported that glaciers in southern Patagonia exhibit one of the fastest rates of mass loss per unit area in the world, where the two largest Northern and Southern Patagonian Icefields are located (Dussaillant et al., 2019; Braun et al., 2019; Hugonnet et al., 2021). The regional mass loss rate during 2000–2018 was estimated to be 0.86 ± 0.27 m w.e. yr^{-1} (Dussaillant et al., 2019), which is nearly double the global mean for mountain glaciers (Hugonnet et al., 2021). The Patagonian Icefields are characterized by large calving outlet glaciers. During 2000–2019, lake-terminating glaciers dominated ice mass loss (lake: 11.2 ± 2.0 Gt a^{-1}; ocean: 2.96 ± 1.19 Gt a^{-1}; land: 1.04 ± 0.31 Gt a^{-1}) (Minowa et al., 2021). This dominance is attributed to their large ablation areas, punctuated by rapid dynamic mass loss events (Sakakibara and Sugiyama, 2014), which are associated with a positive feedback between flow acceleration and ice stretching driven by changes in basal sliding (e.g., Sakakibara et al., 2013). In addition, near-terminus bed topography plays a critical role in the rapid dynamic ice mass loss of freshwater calving glaciers (Sakakibara et al., 2013; Minowa et al., 2023a). Loss of back pressure from the bedrock bump results in dynamic thinning. However, the manner in which recent warming triggers the dynamic mass loss of calving glaciers in this region has poorly been investigated (Sakakibara et al., 2013; Bown et al., 2019; Koch et al.,

* Corresponding author.
E-mail address: m_masa@lowtem.hokudai.ac.jp (M. Minowa).

https://doi.org/10.1016/j.epsl.2026.119930
Received 27 July 2025; Received in revised form 13 January 2026; Accepted 14 February 2026
Available online 26 February 2026

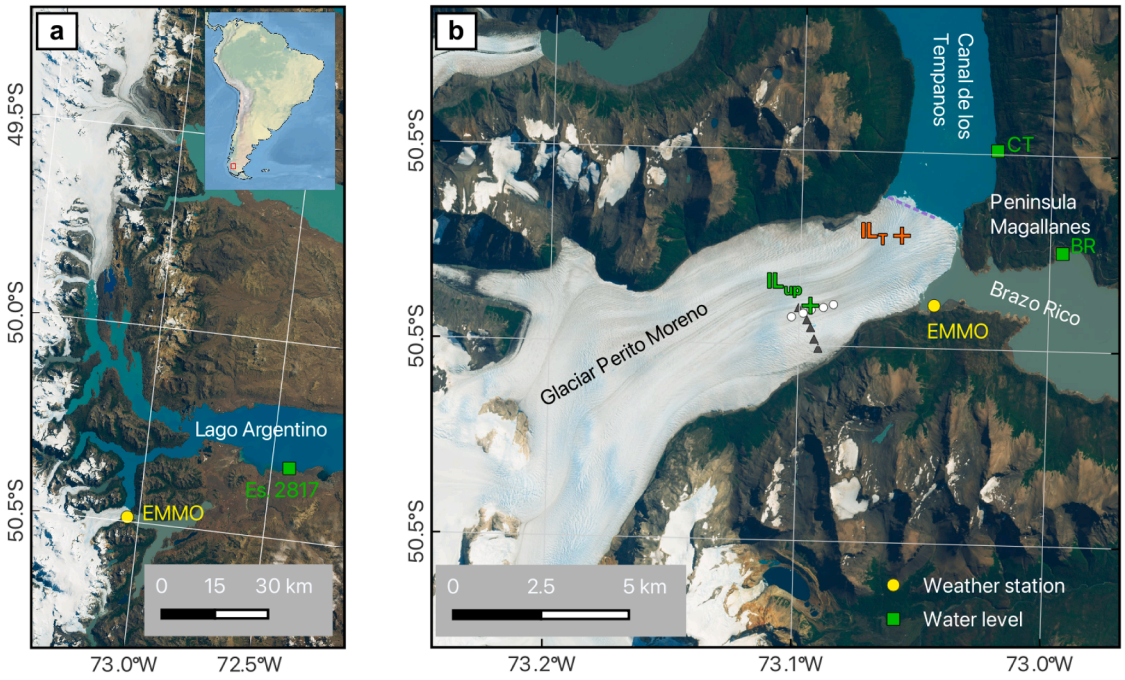

Fig. 1. Map of the study site. **(a)** A satellite map shows the central east part of the southern Patagonian icefield in South America (inset figure). The yellow dot and green squares indicate the location of the weather station and water level gauges, respectively. **(b)** Map of Glaciar Perito Moreno with instrument locations. Satellite-derived flow speed is interpolated at the upper ablation area (green cross) as well as near the terminus (orange cross). Surface elevation has been measured in the lower part of the glacier along the longitudinal (open circles) and transversal points (grey triangles). Surface elevation at the terminus was estimated using ice cliff height along the purple dashed line. The background of both panels is a true colour Sentinel-2A image taken on March 3, 2021.

2025), due to limited field observations and temporally sparse remote sensing datasets.

While most of the glaciers have been retreating in Patagonia, Glaciar Perito Moreno (GPM) has been quasi-stable over the last century (Skvarca and Naruse, 1997). Previous studies have proposed that shallow bedrock topography near the terminus limits the amount of frontal ablation (e.g., Stuefer et al., 2007). In addition, a relatively large accumulation area compared to its ablation area, together with steep terrain at the equilibrium-line altitude, has resulted in limited changes in surface mass balance even under a warming climate (Naruse et al., 1995). Nevertheless, recent observations indicate that GPM has begun to undergo dynamic mass loss in recent years (Koch et al., 2025). Meteorological conditions and point surface mass balance calculated at GPM between 1996 and 2020 (Minowa et al., 2023b) show that the increase in air temperature resulted in a decrease of surface mass balance ranging from −0.4 to −0.9 m w.e. yr^{-1} $decade^{-1}$ near the terminus.

In this study, we aim to articulate the mechanisms that trigger the dynamic ice mass loss of GPM in southern Patagonia (Fig. 1). We analysed changes in ice front position, flow speed and ice surface elevation around the terminus over the last several decades by using high temporal satellite images and geodetic field observations. The recent dynamic retreat of GPM was compared with lake topography, lake level records, and climatic conditions in order to propose triggering mechanisms.

2. Materials and methods

2.1. Satellite image analyses

2.1.1. Terminus position

We analysed 62 scenes of Sentinel-2 A/B optical satellite images to map the ice-front position of GPM between 2020 and 2024. True colour images were composed from orthorectified images to manually delineate the terminus position using the QGIS software. We combined the front position with those previously analysed positions for the period between 1990 and 2019 (Minowa et al., 2021). The error in delineation of the ice-front position ranged from ~14 m for Sentinel 2 images and ~64 m for Landsat 5, evaluated by repeat measurement of the ice front for selected images (Minowa et al., 2021).

2.1.2. Flow speed

Flow speed was interpolated from velocity maps distributed by the ITS_LIVE project (Gardner et al., 2025). Sampling sites were set near the terminus (IL_T) and ablation area of the glacier (IL_{up}) to investigate its temporal variations (Fig. 1). Time separation of image pairs was between 9 and 90 days. A monthly surface speed field was also derived by smoothing individual flow speed data using the LOWESS (LOcally WEighted Scatterplot Smoothing) method (Derkacheva et al., 2020).

2.1.3. Frontal ablation rate

We quantified frontal ablation between 2016 and 2024 using a dense dataset of ice front positions and flow speed, in order to compare it with surface ablation, flow speed, elevation change of surface and lake bathymetry. Frontal ablation a_f is composed of calving rate plus subaqueous melt as:

$$\frac{dL}{dt} = u_m - a_f, \quad (1)$$

where dL/dt is the rate of change in the width-averaged ice front displacement and u_m is width-averaged flow speed near the front. We calculated dL/dt only when the ice front observations were separated >18 days to reduce the uncertainty. u_m was estimated as the 82% of the ice speed at the sampling site at IL_T. The conversion coefficient was derived by computing the mean speed across the terminus in CT using all available measurements. We assumed perfect basal sliding near the glacier terminus. The mean flow speed during the same period was used to derive the frontal ablation rate. The error in frontal ablation ranged between 0.19 and 0.97 m d^{-1}, with a mean error of 0.59 m d^{-1}.

2.1.4. Surface elevation change

The changes in surface elevation are derived from four digital topography maps, including: SRTM (Shuttle Radar Topography Mission) DEM (Digital Elevation Model) v3 acquired February 2000, ALOS/PRISM acquired on March 29, 2008, Pléiades derived DEM acquired on February 2, 2018, and World-View 3 (WV3) derived DEM acquired on April 18, 2020. The Pléiades DEM was available from a previous study with 2-m resolution (Berthier et al., 2024). Stereoscopic optical images taken by ALOS/PRISM and World-View 3 satellites were used to derive DEMs. We utilized the Ames Stereo Pipeline to automatically generate a DEM (Beyer et al., 2018). These three DEMs are co-registered to SRTM with a standard geolocation method (Nuth and Kääb, 2011), which is implemented in an open Python library (Shean et al., 2016). The uncertainties of the DEMs uncertainty was derived from off-glacier stable ground (Table A.1).

2.2. Field observations

2.2.1. GPS-derived surface elevation

Ice surface elevation has been monitored at the lower part of the glacier by a distance meter and theodolite from 1990 and 2013 (Skvarca and Naruse, 1997) (Fig. 1). To extend these early observations, we set up 5 to 6 GPS survey points along and across the glacier since 2013 (Fig. 1). Mean surface elevation change was calculated for transverse and longitudinal profiles. Dual-frequency GPS (Trimble 5800, Trimble Inc. or GEM-1, Enabler Inc.) was placed at each site for 30 min to derive the antenna coordinates with the static method. The accuracy of vertical coordinate was 10 mm.

2.2.2. Lake bathymetry

Lake bathymetry was measured in front of the glacier using a single-beam sonar mounted on a boat in March 2023 and September 2024 (Fig. A.1). We used a depth sounder (HDS-7, Lowrance) operated with an 80 kHz frequency-modulated transducer (Airmar B75M). The horizontal coordinates were obtained by a built-in single-frequency GPS. Water depth, horizontal coordinates and echograms were recorded every 1 s. The uncertainty of the observed depth was estimated in previous studies to be 5.7 m, or 3.7% (Sugiyama et al., 2016). To generate a bathymetry map, we compiled our observations with the early observations (Sugiyama et al., 2016). Finally, irregularly distributed depth data were interpolated into a 50 m grid matrix with a conventional natural neighbouring interpolation method.

We compared our water depth measurements with data taken in December 1998 (Skvarca et al., 2002), for which a 24 Volts hydrographic echo sounder (ECHOTRAC DF 3200 MK II, odom) was operated from an inflatable boat. The instrument depth ranges from 7.5 m to 6000 m, with 0.042% depth accuracy given by the manufacturer. The echo sounder recorded depths at 5-s time intervals, and the continuous echoes were simultaneously recorded each second on thermal paper. The kinematic differential GPS was operated simultaneously and yielded positions with sub-meter accuracy. The change in the lake floor elevation between 1998 and 2023–2024 was calculated at the crossing points within 1 m and interpolated into a 50 m grid matrix. The lake surface level was corrected based on continuous lake level observation in Lago Argentino before calculating the water depth difference (Fig. 1).

2.2.3. Lake water temperature

Lakewater temperature from the surface to the bottom was measured in CT and BR at the inside and outside of the moraine-like bed topography. We lowered a temperature-depth (TD) profiler (COMPACT-TD, JEF Advances Co.) from a boat. We performed measurements twice in CT on April 25, 2023 and September 10, 2024, and once in BR on September 10, 2024. Water temperature was recorded every 1 s while the sensor was lowered to the bottom of the lake. The accuracy of the temperature and depth was $\pm 0.05^{\circ}$C and ±0.3% of the observed depth, respectively.

2.3. Surface mass balance modelling

Specific surface mass balance (SMB) was derived by an energy-balance model and mass-balance model forced with meteorological data obtained at EMMO (Minowa et al., 2023b, 2024). To compare with the surface elevation change in the lower part of the ablation area, we modelled the SMB at that elevation. The calculated specific SMB was compared with stake mass balance measurements carried out near the terminus. The uncertainty of the model was 0.69 m w.e. yr^{-1} (Minowa et al., 2023b). Annual and monthly SMB anomalies were calculated by subtracting the annual mean SMB and mean monthly SMB between 1996 and 2024, respectively. The annual mean was calculated between August 1 and July 31 for the corresponding year.

3. Results and discussion

3.1. The relation between dynamic ice mass loss and enhanced ice melting

Until the year 2018, ice front position, surface elevation and flow speed were relatively stable (Fig. 2(a)–(c)). Thus, GPM has been stable over nearly a century, from the late 1910s when it for the first time reached the shore of Península Magallanes (Skvarca and Naruse, 1997) (Fig. 1(b)). In 2021, a sudden change was observed in the lower part of the glacier (Fig. 2(a)–(c)). The glacier terminus retreat between 2020 and 2024 was seen to be twice as big in CT (390 m) than it was in BR (200 m) (Fig. 2(a)). Flow speed acceleration between 2021 and 2024 was larger at IL_T (2.0 m d^{-1} in 2021 and 2.5 m d^{-1} in 2024) than at IL_{up} (1.4 m d^{-1} in 2021 and 1.7 m d^{-1} in 2024) (Fig. 2(b)). The glacier surface thickened slightly between 1990 and 2004 at a rate of 0.3 m yr^{-1}, then began thinning at 0.6 m yr^{-1} between 2004 and 2017, followed by rapid thinning at about 3.6 m yr^{-1} after 2017 (Fig. 2(c)). These observation, in the frontal retreat, accompanied by accelerated flow speed and surface lowering, suggest that dynamic ice mass loss indeed took place at GPM.

To clarify the triggering mechanisms of dynamic mass-loss, we compared the terminus position, flow speed and surface elevation change with the annual SMB anomaly (Fig. 2(d)). The annual specific SMB anomaly can be divided into three periods (Fig. 2(d)). Between 1996/97 and 2008/09, the SMB anomaly was mostly positive but decreased over time at a rate of −0.18 m w.e. yr^{-2}. The anomaly became negative in 2006/07 (−0.26 m w.e. yr^{-1}) and 2007/08 (−1.55 m w.e. yr^{-1}), respectively (Fig. 2(d)). Between 2009/10 and 2019/20, the SMB was relatively stable, and the anomaly ranged within 1 sigma. Since 2020/21, the SMB anomaly decreased significantly to −1.97 m w.e. yr^{-1} in 2020/21, −2.6 m w.e. yr^{-1} in 2021/22 and −3.4 m w.e. yr^{-1} in 2022/23 hydrological years (Fig. 2(d)). Clearly, onset of the dynamic ice mass loss is synchronized with the significant negative anomalies in SMB. The surface elevation change rate was more than twice as high as the significant negative anomalies in SMB between 2020/21 and 2022/23 (Fig. 2(g)). This confirms that the recent thinning is dominated by glacial dynamics. Such dynamic change in Patagonia, which is often more drastic in nature, has been documented by several studies (e.g., Sakakibara and Sugiyama, 2014), and at calving glaciers in other regions, for example, in Alaska (e.g., O'Neel et al., 2005), in Greenland (e.g., Felikson et al., 2017) and in the Himalayas (e.g., Sato et al., 2022).

The frequent measurements of change in front position (Fig. 2(e)) and flow speed (Fig. 2(g)) analyses enable us to estimate the frontal ablation rate (Fig. 2(h)) based on the Eq. (1), demonstrating that it has increased significantly in March 2021 and successive years up to a maximum of 4 m d^{-1} (Fig. 2(h)). Over those years, the monthly SMB anomaly was strongly negative, particularly in the melting season (Fig. 2(h)). The monthly SMB anomaly became positive in the late 2023 and the early 2024, but the frontal ablation rate was still high. In addition to this distinct transition from stable to unstable glacier fluctuation, we realized a slight retreat of the front position in CT was already beginning

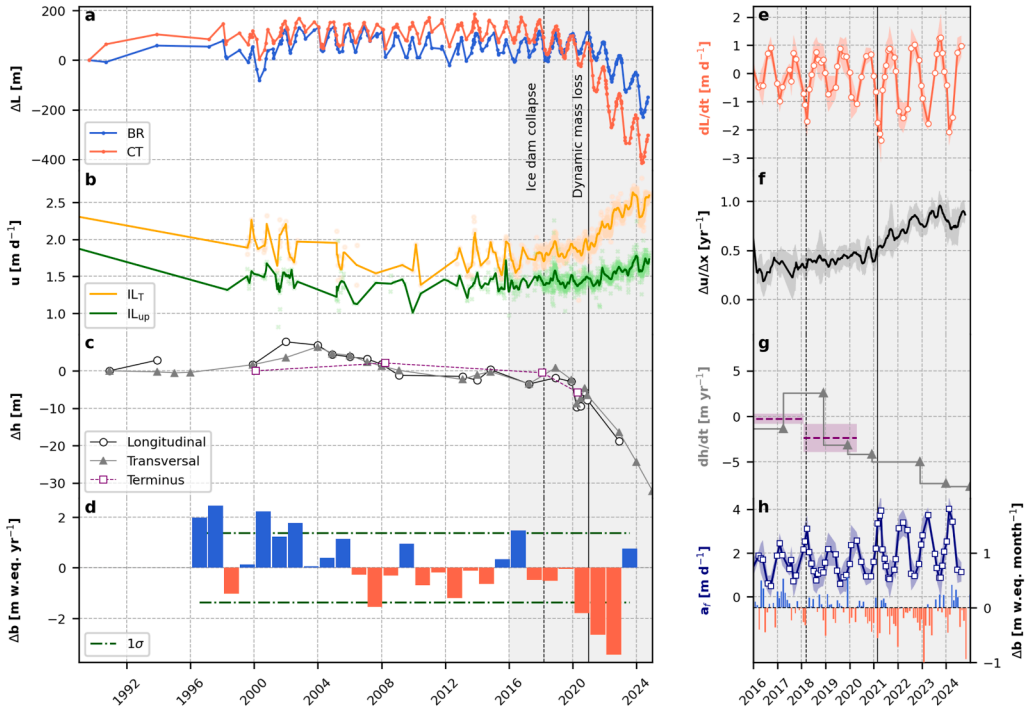

Fig. 2. Glacier fluctuation and specific SMB anomaly time series. **(a)** Ice-front position change (ΔL). Blue and orange lines are the mean relative ice front position in BR and in CT. **(b)** Flow speed (u) obtained from the ITS_LIVE flow speed product at IL_{up} (orange) and IL_T (green) from the ice front (Fig. 1(b)). Coloured markers are individual flow speed measurements, and coloured lines indicate a 60-day moving average of flow speed. **(c)** Relative surface elevation (Δh) since the initial measurement along longitudinal (open circle) and transversal (open triangle) survey points (Fig. 1(b)). The purple squares indicate the mean surface elevation along the ice front taken from the DEMs (Fig. 1(b)). **(d)** Blue and red bars indicate annual point SMB anomaly (Δb) forced by the meteorological conditions at EMMO (Fig. 1(b)). **(e)** Rate of ice front displacement in CT (dL/dt). **(f)** The flow speed gradient is calculated between IL_T and IL_{up}. **(g)** Surface elevation change rate (dh/dt) is calculated from transverse survey points. Purple dashed horizontal line is the elevation change rate near the terminus. **(h)** Frontal ablation rate (a_f) for the ice front in CT. Blue and red bars indicate monthly SMB anomaly (Δb). Black dashed and solid vertical lines throughout the panels highlight the dates when the ice dam collapsed (Fig. A.2) and dynamic ice mass-loss became evident, respectively.

in March 2018 (Fig. 2(a) and (e)), when the terminus displacement rate reached $-1.7 \pm 0.5\,m\,d^{-1}$ (Fig. 2(e)). The front position advanced over the following winter and spring but did not reached the most advanced positions seen in the previous years (Fig. 2(a) and (e)). This slight annual retreat continued until 2020 (Fig. 2(a)) before the large retreat occurring in March 2021 (Fig. 2(e)). The frontal ablation rate of March 2018 reached $3.0 \pm 0.7\,m\,d^{-1}$ (Fig. 2(h)). The mean monthly SMB anomaly suggests a slightly negative SMB in the melt season of 2017/18, but not as negative as in the year 2020/21 (Fig. 2(h)).

Before discussing the potential connections between the negative SMB and the dynamic mass loss, we will describe the spatial patterns of the changes in surface elevation, flow speed and terminus positions before and after 2018 (Fig. 3). The upper portion of the glacier (above 2 km from the terminus) showed surface lowering between 2000 and 2008, whereas the ice surface elevation increased near the terminus (Figs. 3(a) and A.3). The surface elevation was slightly more increased (0.5 m on average) than the lower ablation area between 2008 and 2018 (Fig. 3(b)). In contrast, the surface elevation lowered by 6.3 ± 3.9 m on average all over the lower ablation area between 2018 and 2020 (Figs. 3(c) and A.3). Monthly averaged surface flow speed anomalies indicate that only slight flow acceleration can be observed near the front in March 2018 (Fig. 3(d)), whereas the flow speed significantly increased near the terminus after March 2020, particularly where the glacier flows into CT (Fig. 3(e) and (f)). Additionally, the flow acceleration propagates upglacier over time (Fig. 3(e) and (f)). We realized that frontal retreat had occurred along the ice front in March 2018, particularly at the tip of the ice front (Fig. 3(d)). Whereas, in both 2020 and 2021, the majority of the frontal retreat was observed along the terminus in CT (Fig. 3(e) and (f)).

3.2. Influence of the morainal bank on glacier dynamics

Lake topography was measured over the region where the ice front has retreated since 2018 (Fig. 4(a)). In CT and BR, shallow water depths were measured across the lake in front of the termini, where the ice fronts have been located for the past century. In CT, the water depth decreases sharply from the lake towards the glacier terminus, from ~180 m to 50–90 m (Fig. 4(a) and (c)). In BR, depths similarly decreased from ~110 m to 30–60 m near the terminus (Fig. 4(a) and (d)). In both CT and BR, thick sediment layers were identified with seismic profiling near the terminus (Lodolo et al., 2020). We therefore speculate that the elevated topography represents a subaqueous morainal bank that developed, at least in part, as a result of the glacier's advance since 1917 (Skvarca and Naruse, 1997). This advance postdates the latest Little Ice Age advance at ca. 1820–1850, inferred from C-14 dating of wood and organic samples (Aniya and Skvarca, 2012).

The shallow water depths associated with this morainal bank likely acted as a pinning point, stabilizing the ice front by increasing resistive stress and limiting calving for much of the twentieth century. Water depth increased towards the glacier from the morainal bank (Fig. 4(a)), such that once the ice front retreated off the morainal bank and into deeper water, this stabilizing effect was progressively lost. This transition is crucial for enhancing calving as the ice front retreat into deeper water by increasing buoyancy force, flow speed by increasing subglacial water pressure near the terminus, as well as loss of back stress against the driving stress (Benn et al., 2007). The ice front retreated the most in 2021, and the mean water depth along the ice front of CT increased from 119 m on May 12, 2020, to 129 m on May 10, 2021. This was the critical change needed to initiate the following dynamic retreat of the

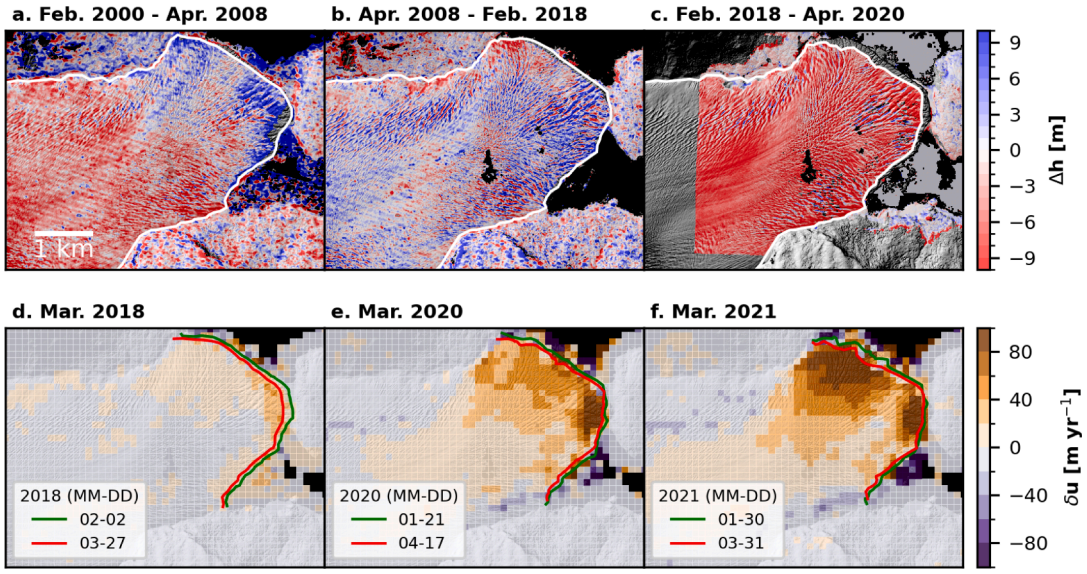

Fig. 3. Spatial changes in surface ice elevation and flow speed anomaly. The changes in surface elevation between **(a)** February 2000 and April 2008, **(b)** April 2008 and February 2018, and **(c)** February 2018 and April 2020, respectively. The white line indicates the glacier extent. The monthly flow speed field anomaly for **(d)** March 2018, **(e)** March 2020, and **(f)** March 2021 relative to the mean annual flow speed between August 2017 and July 2018. The background image is a hillshade made from the Pléiades DEM in 2018.

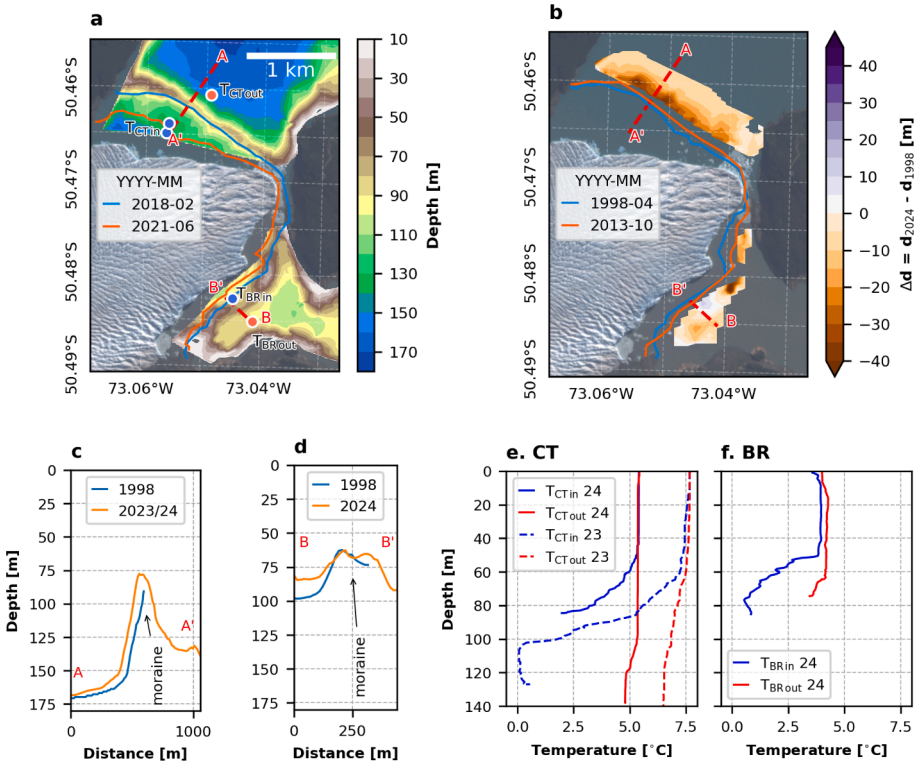

Fig. 4. **(a)** Bathymetry map in front of Glaciar Perito Moreno generated by data obtained in 2012 and 2023/24. Colour contours show the water depths. The ice front positions in February 2018 and June 2021 are shown. Blue and red circles indicate the location of a temperature profile sensor lowered into the lake inside and outside of the moraine. **(b)** Change in water depth between 1998 and 2023/24. Blue and orange lines indicate the ice front position on April 14, 1998, and October 15, 2013, respectively. The cross-sectional profile of water depth in **(c)** 1998 and 2023/24 along A–A' and **(d)** 1998 and 2024 along B–B'. The transects are indicated in panels **(a)** and **(b)**. Water temperature profiles observed on April 25, 2023 and September 10, 2024 **(e)** in CT and **(f)** in BR. Water temperature was measured inside and outside of the moraine (Fig. 4(a)).

glacier, accompanied by the significant negative surface mass balance (Fig. 2).

GPM had been stable while most of the other calving glaciers were retreating in the region (e.g., Sakakibara and Sugiyama, 2014) even under the atmospheric warming conditions (Minowa et al., 2023b), most likely because the morainal bank maintained shallow water depths and sustained frontal pinning (Fig. 4(a)). Among the freshwater calving glaciers located on the eastern side of the Southern Patagonian Icefield, the GPM has one of the shallowest depths (61 m deep on average), whereas those near the front of the glaciers in the year 2001 were 201 m for

Glaciar O'higgins, 177 m for Glaciar Viedma, 384 m for Glaciar Upsala and 170 m for Glaciar Tyndall (Minowa et al., 2023a). Therefore, the GPM flows into a lake 2–6 times shallower, when compared to other glaciers, which limits calving and flow, and delays the retreat of the glacier. In addition to this, repeat water depth measurements in 1998 and 2023/24 shows the morainal bank growth and a decrease in water depth (Fig. 4(b)). The water depth decreased by 14.5 m in CT and 5.5 m in BR on average (Fig. 4(b)). In particular, decreased water depth from 1998 to 2024 was observed near the terminus of the glacier in CT (Fig. 4(b) and (c)). Decreased water depth near the morainal bank was 40 m (equivalent to 1.5 m yr^{-1}), while that over the flatter part of the lake was 8 m (equivalent to 0.3 m yr^{-1}). Because the ice front has remained in quasi-equilibrium over recent decades, continued delivery of subglacial sediment can lead to growth of a sediment bank. In addition, the maximum ice-front extent was observed in 2013 and was accompanied by a seasonal cycle of ice-front retreat and advance (Fig. 2(a)). We therefore suggest that the larger decrease in water depth near the terminus is partly due to expansion of the subaqueous moraine driven by repeated seasonal interaction between the glacier front and the sediment. Turbid subglacial discharge has been observed in the Patagonian pro-glacial lakes (Sugiyama et al., 2016). Even more discharge under a warming climate will increase the sedimentation rate, which facilitates development of morainal bank (Brinkerhoff et al., 2017). Similar stabilizing effects and delayed retreat due to development of a morainal bank have been observed in many tidewater glaciers in Alaska (Goff et al., 2012; Eidam et al., 2020).

Moraine may also modulate frontal ablation by reducing the subaqueous melt rate. Water temperature showed clear differences inside and outside of the moraine in CT and BR (Fig. 4(a), (e), and (f)). While temperatures are similar around 50 m in profiles both inside and outside of the moraine, the temperature below that depth showed significantly lower temperature only inside the moraine in both lakes, particularly in the melt season due to an increase in meltwater discharge (Fig. 4(e) and (f)). Cold water remains in deep because sediment-laden subglacial discharge is denser than lake water (Sugiyama et al., 2016). The cold water may limit the subaqueous melt rate and help ice foot formation within the lake. Whereas subaqueous melt rate decreases frontal ablation due to the cold temperature, the subaqueous ice foot development causes additional buoyant force acting on the ice cliff and can cause full-thickness large iceberg calving of large icebergs (e.g., Trevers et al., 2019). The influence of contrasting lake temperature structures on overall frontal ablation warrants further investigation.

3.3. Triggering mechanisms of the dynamic mass loss

The relationship between calving glacier changes and recent climate change often shows high complexity, making prediction of calving glaciers uncertain (Marzeion et al., 2020). Our results indicate that the gradually decreasing trends in SMB and surface elevation since the mid-2000s may have resulted in the ice thinning, flow acceleration and terminus retreat initiated in 2018 (Fig. 2(b) and (c)). The decreasing trend in SMB is dominated by the atmospheric warming in the region (Minowa et al., 2023b). Borehole measurements in the lower ablation area of GPM revealed that subglacial water pressure was about 95% of ice overburden pressure (Sugiyama et al., 2011). The short-term flow speed variations of GPM are closely in phase with meltwater input, which modulates basal water pressure. Thus, the long-term gradual thinning results in the glacier being closer to a floating condition near the terminus and might enhance flow speed by increasing basal sliding (Figs. 2 and 3). The longitudinal strain rate in the lower part of the glacier has increased gradually from 0.4 to 0.5 yr^{-1} between 2018 and 2020 (Fig. 2(f)). This suggests the glacier has already started the dynamic mass loss in 2018.

Interestingly, a connection was seen between the gradual recession of GPM and the ice dam collapse in March 2018 (Figs. 2 and A.2). The ice dam collapse occurred on March 11, 2018 and the water level dropped by 10.4 m in BR, consequently rising the water level in CT by 2.0 m (Fig. A.2). This is one of the most significant ice damming events over the past half century due to a channel closure between the front and Península Magallanes (Figs. 1(b) and A.2). The ice front retreated at the tip of the front and the terminus both in CT and BR in March 2018 (Fig. 3(d)). Such water level changes may not be a critical change in the buoyancy force to increase the calving event because the ice front in the both parts of the lake are well grounded (Fig. A.4). However, even small changes in the water level can cause an increase in the subglacial water pressure near the terminus, which may enhanced basal sliding and extensional flow (Podolskiy et al., 2016). More fractures and calving can be expected for enhanced extensional flow (e.g., Benn et al., 2007).

The spatiotemporal variation of the surface elevation and flow speed of GPM and the SMB variability suggests that the significantly negative SMB since 2020/21 might have triggered the distinct dynamic mass loss of the glacier (Fig. 2). Atmospheric warming not only accelerates negative SMB but also would enhance subaerial calving events by subaqueous melting due to warmed lake surface (Minowa et al., 2017) and followed by remaining subaqueous iceberg break-up as a relatively large buoyancy-driven calving event (Trevers et al., 2019; Sugiyama et al., 2019). The enhanced frontal ablation resulted in the ice front's retreat from the shallow water at the morainal bank into a deeper lake (Fig. 4(a)). It further increases the buoyancy force acting on the ice cliff, resulting in large-scale calving events. The loss of back pressure from the morainal bank also results in a drastic increase in flow speed and stretching flow by changing stress balance (Fig. 2(b) and (f)). More frequent calving events are expected in such a high stretching flow regime, and the ice front will retreat further (Fig. 2(h)).

The potential triggers of dynamic mass loss identified in this study may have several implications for the future stability of lake-terminating sectors of the Greenland Ice Sheet (How et al., 2021; Carrivick et al., 2022). Currently, about 10% of the ice-sheet margin is occupied by marginal lakes, where ice flow speeds are approximately 25% higher than along land-terminating margins (Carrivick et al., 2022). Although ice discharge into lakes accounts for only about 1% of the total discharge to the ocean, relative importance of lake-terminating margins are expected to increase in the future as the ice-sheet margin continues to retreat and many marine termini transition to land-terminating configurations (Carrivick et al., 2022). Continued climate warming, punctuated by episodic extreme heat waves, is expected in the coming decades (e.g., Perkins-Kirkpatrick and Lewis, 2020). Such atmospheric forcing may trigger dynamic ice-mass loss in lake-terminating sectors dependent on their bed topography, further enhancing future mass loss from the ice sheet. In addition, recent satellite altimetry has revealed active water-level changes in marginal lakes (Dømgaard et al., 2024). That study monitored more than 1100 lakes out of over 3300 marginal lakes around the Greenland Ice Sheet. Nearly half of the monitored lakes exhibited rapid drainage followed by gradual refilling, particularly during the high-melt year of 2019 (Dømgaard et al., 2024). Our results suggest that even small variations in lake level can influence basal sliding near glacier terminus, resulted in the mass loss of freshwater-calving glacier. Ongoing changes occurring around the ice-sheet margin will influence its future evolution. Further analyses using numerical frontal-ablation and ice-flow modelling, combined with field observations, will help to clarify the full cascade of processes operating under warming conditions and improve projections of the behaviour of these complex freshwater-calving glacier systems.

4. Conclusion

We documented the recent unstable behaviour of Glaciar Perito Moreno, a freshwater-calving glacier in southern Patagonia that had remained stable for 100 years, even in the face of a warming climate. We combined a long-term field dataset with satellite observations and additional field measurements, including lake bathymetry. We show that atmospheric warming and sustained ice thinning over recent decades triggered a gradual increase in flow speed near the terminus, ultimately

initiating the dynamic ice-mass loss that began in 2018. We also pointed out the potential impact of the ice dam collapse in 2018, which enhanced calving activity and resulted in the net terminus retreat. Unlike other Patagonian glaciers, GPM had been stable because of its shallow bathymetry due to the morainal bank developed in front of the glacier, which delayed glacier retreat by reducing calving and providing resistive stress. Three melt seasons between 2020/21 and 2022/23 were striking to increase in frontal ablation, causing the ice front to retreat from the morainal bank. This changed the stress balance of the glacier and contributed to the substantial flow acceleration and dynamic ice mass loss.

Data Availability

Data presented in this study is available from the data repository upon publication (https://doi.org/10.5281/zenodo.18167474). Remote sensing datasets were downloaded from public data repositories: SRTM DEM (https://earthexplorer.usgs.gov/), Pléiade DEM (https://en.poleterresolide.fr/data-access), Sentinel-2A/B (https://browser.dataspace.copernicus.eu/), and the ITS_LIVE flow speed product (https://its-live.jpl.nasa.gov/). The water level record of Lago Argentino (Estación 2817-Calafate) is available at Sistema Nacional de Información Hídrica (https://snih.hidricosargentina.gob.ar)

Authors Contribution

MM performed data processing, participated in fieldwork, and wrote the manuscript. PS maintained the instruments, coordinated field activities and provided long-term records. KF developed the surface mass balance model. NN performed the GPS ice surface elevation measurement in 2009, 2013 and 2014. All authors discussed the material presented in the paper at each stage of data processing and have contributed to prepare the final manuscript.

CRediT authorship contribution statement

Masahiro Minowa: Writing – review & editing, Writing – original draft, Visualization, Validation, Software, Resources, Project administration, Methodology, Investigation, Funding acquisition, Formal analysis, Data curation, Conceptualization; **Pedro Skvarca:** Writing – review & editing, Project administration, Data curation; **Koji Fujita:** Writing – review & editing, Software, Methodology; **Nozomu Naito:** Writing – review & editing, Data curation; **Shin Sugiyama:** Writing – review & editing.

Declaration of competing interest

We have no conflicts of interest to disclose.

Acknowledgements

We are grateful to those who helped in field observations, in particular to Carlos Domínguez and Steffen Welsch, as well as other guides and park rangers. Thanks are due to Intendencia Parque Nacional los Glaciares for their support in lake measurements and Hielo y Aventura for logistic facilities. Many thanks to all who have contributed to GRPP (Glacier Research Project in Patagonia) over the decades. We also thank Shigeru Aoki for lending the water temperature profiler. English text was corrected by Ariah Kidder. The study was supported by JSPS KAKENHI Grant 22K14093 and 25H00425. Field activities were carried out within the Project No. 089, DRPA, Administración de Parques Nacionales, Argentina. Datasets were analyzed with Python 3.11. Figures were produced by Python 3.11 and QGIS3.

Appendix A. Lake water level

Water level of Lago Argentino was measured at El Calafate (Estación 2817 in LA in Fig. 1(a)), from 1992–2024. It was tied to the first order accuracy (mm) leveling linked to the Argentine sea level gauge Datum. GEOIDE-Ar16, the latest National Vertical Reference adjusted and adopted by Argentina in 2016. In addition to this, water level has been measured at the shore of Canal de los Témpanos (CT) and Brazo Rico (BR) with a water pressure sensor (HOBO CO-U20-001) with an accuracy of ±1.5 cm (CT and BR in Fig. 1). We used part of the data recorded during the periods between January 2017 and October 2018 in CT and between March 2017 and April 2018 in BR.

Table A.1
The median difference (MD) and normalized median absolute deviations (NMAD) over stable bedrock.

DEMs	MD [m]	NMAD [m]
SRTM—ALOS	0.42	7.75
SRTM—Pléiades,	−0.02	5.49
SRTM—WV3	−0.33	3.93
ALOS—Pléiades	−0.02	4.05
Pléiades–WV3	0.0	0.88

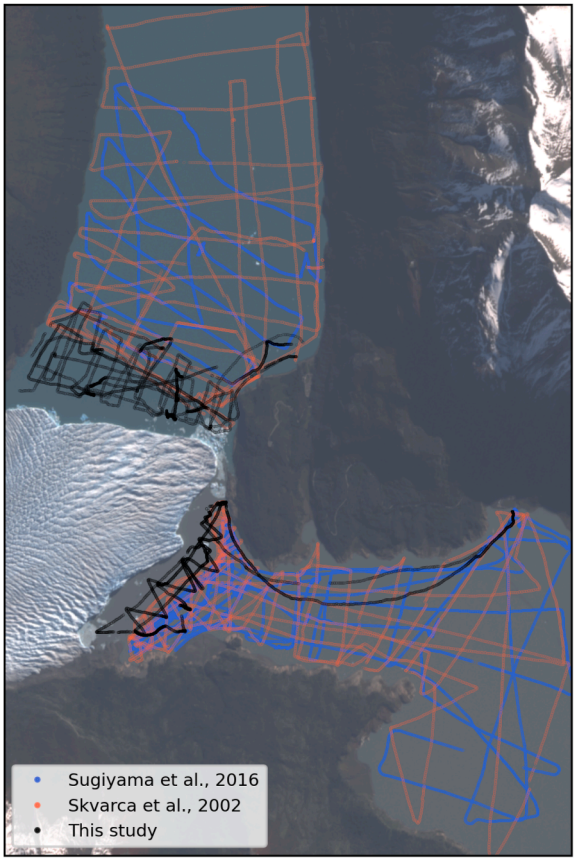

Fig. A.1. Water depth survey tracks.

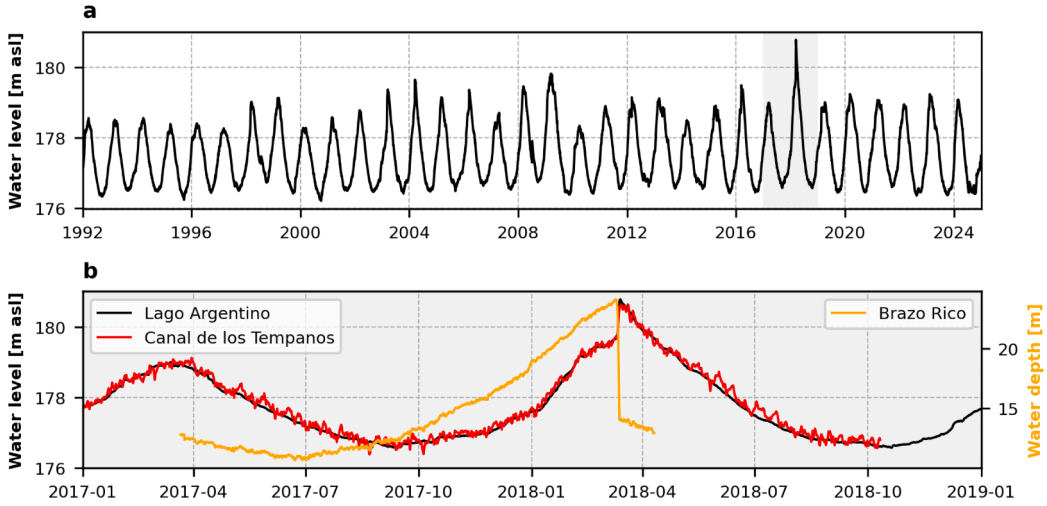

Fig. A.2. **(a)** Water level of Lago Argentino between 1992 and 2024. **(b)** Water levels observed during the ice dam collapse occurred in March 2018.

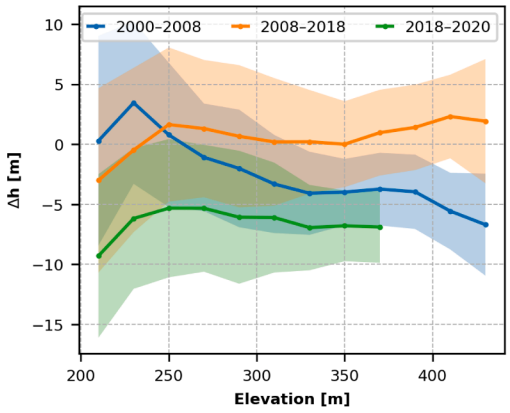

Fig. A.3. Ice surface elevation change vs. ice elevation. The mean elevation change is calculated for each 20 m elevation bin. Coloured areas indicate one standard deviation of elevation change for each elevation bin.

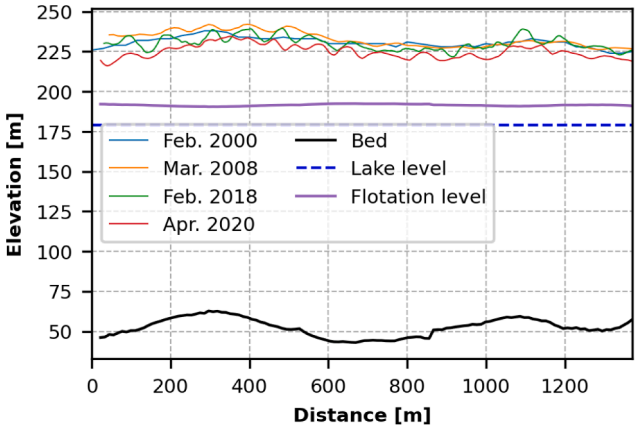

Fig. A.4. Cross-sectional profile of ice surface elevation near the terminus of CT, obtained from the four DEMs. The profile is indicated in Fig. 1(b). The lake topography (black line) and flotation level (purple line) along the same transect line are also indicated.

References

Aniya, M., Skvarca, P., 2012. Little ice age advances of Glaciar Perito Moreno, Hielo Patagónico Sur, South America. Bull. Glacier Res. 30, 1–8. https://doi.org/10.5331/bgr.30.1

Benn, D.I., Warren, C.R., Mottram, R.H., 2007. Calving processes and the dynamics of calving glaciers. Earth-Sci. Rev. 82 (3-4), 143–179. https://doi.org/10.1016/j.earscirev.2007.02.002

Berthier, E., Lebreton, J., Fontannaz, D., Hosford, S., Belart, J. M.-C., Brun, F., Andreassen, L.M., Menounos, B., Blondel, C., 2024. The Pléiades Glacier observatory: high-resolution digital elevation models and ortho-imagery to monitor glacier change. Cryosphere 18 (12), 5551–5571. https://doi.org/10.5194/tc-18-5551-2024

Beyer, R.A., Alexandrov, O., McMichael, S., 2018. The Ames Stereo pipeline: NASA's open source software for deriving and processing terrain data. Earth Space Sci. 5 (9), 537–548. https://doi.org/10.1029/2018EA000409

Bown, F., Rivera, A., Pętlicki, M., Bravo, C., Oberreuter, J., Moffat, C., 2019. Recent ice dynamics and mass balance of Jorge Montt Glacier, Southern Patagonia icefield. J. Glaciol. 65 (253), 732–744. https://doi.org/10.1017/jog.2019.47

Braun, M.H., Malz, P., Sommer, C., Farías-Barahona, D., Sauter, T., Casassa, G., Soruco, A., Skvarca, P., Seehaus, T.C., 2019. Constraining glacier elevation and mass changes in South America. Nat. Clim. Chang. 9 (2), 130–136. https://doi.org/10.1038/s41558-018-0375-7

Brinkerhoff, D., Truffer, M., Aschwanden, A., 2017. Sediment transport drives tidewater glacier periodicity. Nat. Comm. 8 (1), 90. https://doi.org/10.1038/s41467-017-00095-5

Carrivick, J.L., How, P., Lea, J.M., Sutherland, J.L., Grimes, M., Tweed, F.S., Cornford, S., Quincey, D.J., Mallalieu, J., 2022. Ice-marginal proglacial lakes across greenland: present status and a possible future. Geophys. Res. Lett. 49 (12), e2022GL099276. https://doi.org/10.1029/2022GL099276

Cowton, T.R., Sole, A.J., Nienow, P.W., Slater, D.A., Christoffersen, P., 2018. Linear response of east greenland's tidewater glaciers to ocean/atmosphere warming. Proc. Natl. Acad. Sci. 115 (31), 7907–7912. https://doi.org/10.1073/pnas.1801769115

Derkacheva, A., Mouginot, J., Millan, R., Maier, N., Gillet-Chaulet, F., 2020. Data reduction using statistical and regression approaches for ice velocity derived by landsat-8, sentinel-1 and sentinel-2. Remote Sens. 12 (12), 1935. https://doi.org/10.3390/rs12121935

Dømgaard, M., Kjeldsen, K., How, P., Bjørk, A., 2024. Altimetry-based ice-marginal lake water level changes in greenland. Commun. Earth Environ. 5 (1), 365. https://doi.org/10.1038/s43247-024-01522-4

Dussaillant, I., Berthier, E., Brun, F., Masiokas, M., Hugonnet, R., Favier, V., Rabatel, A., Pitte, P., Ruiz, L., 2019. Two decades of glacier mass loss along the Andes. Nat. Geosci. 12, 802–808. https://doi.org/10.1038/s41561-019-0432-5

Eidam, E.F., Sutherland, D.A., Duncan, D., Kienholz, C., Amundson, J.M., Motyka, R.J., 2020. Morainal bank evolution and impact on terminus dynamics during a tidewater glacier stillstand. J. Geophys. Res.-Earth 125 (11), e2019JF005359. https://doi.org/10.1029/2019JF005359

Felikson, D., Bartholomaus, T.C., Catania, G.A., Korsgaard, N.J., Kjær, K.H., Morlighem, M., Noël, B., Van Den Broeke, M., Stearns, L.A., Shroyer, E.L., Sutherland, D.A., Nash, J.D., 2017. Inland thinning on the greenland ice sheet controlled by outlet glacier geometry. Nat. Geosci. 10 (5), 366–369. https://doi.org/10.1038/ngeo2934

Foss, Ø., Maton, J., Moholdt, G., Schmidt, L.S., Sutherland, D.A., Fer, I., Nilsen, F., Kohler, J., Sundfjord, A., 2024. Ocean warming drives immediate mass loss from calving glaciers in the high Arctic. Nat. Comm. 15 (1), 1–9. https://doi.org/10.1038/s41467-024-54825-7

Gardner, A.S., Greene, C.A., Kennedy, J.H., Fahnestock, M.A., Liukis, M., López, L.A., Lei, Y., Scambos, T.A., Dehecq, A., 2025. ITS_LIVE global glacier velocity data in near-real time. Cryosphere 19 (9), 3517–3533. https://doi.org/10.5194/tc-19-3517-2025

Goff, J.A., Lawson, D.E., Willems, B.A., Davis, M., Gulick, S. P.S., 2012. Morainal bank progradation and sediment accumulation in disenchantment Bay, Alaska: response to advancing Hubbard Glacier. J. Geophys. Res. Earth Surf. 117 (2), F02031. https://doi.org/10.1029/2011JF002312

How, P., Messerli, A., Mätzler, E., Santoro, M., Wiesmann, A., Caduff, R., Langley, K., Bojesen, M.H., Paul, F., Kääb, A., et al., 2021. Greenland-wide inventory of ice marginal lakes using a multi-method approach. Sci. Rep. 11 (1), 4481. https://doi.org/10.1038/s41598-021-83509-1

Hugonnet, R., McNabb, R., Berthier, E., Menounos, B., Nuth, C., Girod, L., Farinotti, D., Huss, M., Dussaillant, I., Brun, F., et al., 2021. Accelerated global glacier mass loss in the early twenty-first century. Nature 592 (7856), 726–731. https://doi.org/10.1038/s41586-021-03436-z

Koch, M., Sommer, C., Blindow, N., Lutz, K., Skvarca, P., Ruiz, L., Rizzoli, P., Bueso-Bello, J.-L., Fürst, J.J., Braun, M.H., 2025. The state and fate of Glaciar Perito Moreno Patagonia. Commun. Earth Environ. 6 (1). https://doi.org/10.1038/s43247-025-02515-7

Lodolo, E., Donda, F., Lozano, J., Baradello, L., Romeo, R., Bran, D.M., Tassone, A., 2020. The submerged footprint of Perito Moreno Glacier. Sci. Rep. 10 (1), 16437. https://doi.org/10.1038/s41598-020-73410-8

Marzeion, B., Hock, R., Anderson, B., Bliss, A., Champollion, N., Fujita, K., Huss, M., Immerzeel, W.W., Kraaijenbrink, P., Malles, J.-H., et al., 2020. Partitioning the uncertainty of ensemble projections of global glacier mass change. Earth's Future 8 (7), e2019EF001470. https://doi.org/10.1029/2019EF001470

Minowa, M., Schaefer, M., Skvarca, P., 2023a. Effects of topography on dynamics and mass loss of lake-terminating glaciers in Southern Patagonia. J. Glaciol. 69 (278), 1580–1597. https://doi.org/10.1017/jog.2023.42

Minowa, M., Schaefer, M., Sugiyama, S., Sakakibara, D., Skvarca, P., 2021. Frontal ablation and mass loss of the Patagonian icefields. Earth Planet. Sci. Lett. 561, 116811. https://doi.org/10.1016/j.epsl.2021.116811

Minowa, M., Skvarca, P., Fujita, K., 2023b. Climate and surface mass balance at Glaciar Perito Moreno, Southern Patagonia. J. Clim. 36 (2), 625–641. https://doi.org/10.1175/JCLI-D-22-0294.1

Minowa, M., Skvarca, P., Fujita, K., 2024. Foehn winds influence surface ablation on Glaciar Perito Moreno, Southern Patagonian icefield. J. Glaciol. 70, e40. https://doi.org/10.1017/jog.2023.106

Minowa, M., Sugiyama, S., Sakakibara, D., Skvarca, P., 2017. Seasonal variations in ice-front position controlled by frontal ablation at Glaciar Perito Moreno, the Southern Patagonia icefield. Front. Earth Sci. 5 (January), 1–15. https://doi.org/10.3389/feart.2017.00001

Naruse, R., Aniya, M., Skvarca, P., Gasassa, G., 1995. Recent variations of calving glaciers in Patagonia, South America, revealed by ground surveys, satellite-data analyses and numerical experiments. Ann. Glaciol. 21, 297–303. https://doi.org/10.3189/S0260305500015974

Nuth, C., Kääb, A., 2011. Co-registration and bias corrections of satellite elevation data sets for quantifying glacier thickness change. Cryosphere 5 (1), 271–290. https://doi.org/10.5194/tc-5-271-2011

O'Neel, S., Pfeffer, W.T., Krimmel, R., Meier, M., 2005. Evolving force balance at Columbia Glacier, Alaska, during its rapid retreat. J. Geophys. Res.-Earth 110 (F3). https://doi.org/10.1029/2005JF000292

Otosaka, I.N., Shepherd, A., Ivins, E.R., Schlegel, N.-J., Amory, C., van den Broeke, M., Horwath, M., Joughin, I., King, M., Krinner, G., et al., 2023. Mass balance of the greenland and Antarctic ice sheets from 1992 to 2020. Earth Syst. Sci. Data 15 (4), 1597–1616. https://doi.org/10.5194/essd-15-1597-2023

Perkins-Kirkpatrick, S.E., Lewis, S.C., 2020. Increasing trends in regional heatwaves. Nat. Commun. 11 (1), 3357. https://doi.org/10.1038/s41467-020-16970-7

Podolskiy, E.A., Sugiyama, S., Funk, M., Walter, F., Genco, R., Tsutaki, S., Minowa, M., Ripepe, M., 2016. Tide-modulated ice flow variations drive seismicity near the calving front of Bowdoin Glacier, greenland. Geophys. Res. Lett. 43 (5), 2036–2044. https://doi.org/10.1002/2016GL067743

Rounce, D.R., Hock, R., Maussion, F., Hugonnet, R., Kochtitzky, W., Huss, M., Berthier, E., Brinkerhoff, D., Compagno, L., Copland, L., et al., 2023. Global glacier change in the 21st century: every increase in temperature matters. Science 379 (6627), 78–83. https://doi.org/10.1126/science.abo1324

Sakakibara, D., Sugiyama, S., 2014. Ice-front variations and speed changes of calving glaciers in the Southern Patagonia icefield from 1984 to 2011. J. Geophys. Res.-Earth 119 (11), 2541–2554. https://doi.org/10.1002/2014JF003148

Sakakibara, D., Sugiyama, S., Sawagaki, T., Marinsek, S., Skvarca, P., 2013. Rapid retreat, acceleration and thinning of Glaciar Upsala, Southern Patagonia icefield, initiated in 2008. Ann. Glaciol. 54 (63), 131–138. https://doi.org/10.3189/2013AoG63A236

Sato, Y., Fujita, K., Inoue, H., Sakai, A., Karma, 2022. Land- to lake-terminating transition triggers dynamic thinning of a Bhutanese Glacier. Cryosphere 16 (6), 2643–2654. https://doi.org/10.5194/tc-16-2643-2022

Shean, D.E., Alexandrov, O., Moratto, Z.M., Smith, B.E., Joughin, I.R., Porter, C., Morin, P., 2016. An automated, open-source pipeline for mass production of digital elevation models (DEMs) from very-high-resolution commercial stereo satellite imagery. ISPRS J. Photogramm. Remote Sens. 116, 101–117. https://doi.org/10.1016/j.isprsjprs.2016.03.012

Skvarca, P., De Ángelis, H., Naruse, R., Warren, C.R., Aniya, M., 2002. Calving rates in fresh water : new data from southern Patagonia. Ann. Glaciol. 34:1, 379–384. https://doi.org/10.3189/172756402781817806

Skvarca, P., Naruse, R., 1997. Dynamic behavior of Glaciar Perito Moreno, Southern Patagonia. Ann. Glaciol. 24, 268–271. https://doi.org/10.3189/S0260305500012283

Stuefer, M., Rott, H., Skvarca, P., 2007. Glaciar Perito Moreno, Patagonia: climate sensitivities and glacier characteristics preceding the 2003/04 and 2005/06 damming events. J. Glaciol. 53 (180), 3–16. https://doi.org/10.3189/172756507781833848

Sugiyama, S., Minowa, M., Sakakibara, D., Skvarca, P., Sawagaki, T., Ohashi, Y., Naito, N., Chikita, K., 2016. Thermal structure of proglacial lakes in Patagonia. J. Geophys. Res.-Earth 121 (12), 2270–2286. https://doi.org/10.1002/2016JF004084

Sugiyama, S., Minowa, M., Schaefer, M., 2019. Underwater ice terrace observed at the front of Glaciar grey, a freshwater calving glacier in Patagonia. Geophys. Res. Lett. 46 (5), 2602–2609. https://doi.org/10.1029/2018GL081441

Sugiyama, S., Skvarca, P., Naito, N., Enomoto, H., Tsutaki, S., Tone, K., Marinsek, S., Aniya, M., 2011. Ice speed of a calving glacier modulated by small fluctuations in basal water pressure. Nat. Geosci. 4 (9), 597–600. https://doi.org/10.1038/ngeo1218

Trevers, M., Payne, A.J., Cornford, S.L., Moon, T., 2019. Buoyant forces promote tidewater glacier iceberg calving through large basal stress concentrations. Cryosphere 13 (7), 1877–1887. https://doi.org/10.5194/tc-13-1877-2019

Truffer, M., Motyka, R., 2016. Where glaciers meet water: subaqueous melt and its relevance to glaciers in various settings. Rev. Geophys. 54, 220–239. https://doi.org/10.1002/2015RG000494